3D Mapping and Stability Prediction for Autonomous Wheelchairs

Aryan Naveen, Haitao Luo, Zhimin Chen, Bing Li
Department of Automotive Engineering, Clemson University
International Center for Automotive Research (CU-ICAR), Email: bli4@clemson.edu

CLEMSON UNIVERSITY INTERNATIONAL CENTER FOR AUTOMOTIVE RESEARCH

I. Introduction

Autonomous wheelchairs can address broad needs in many populations by serving as the gateway to a much higher degree of independence and mobility capability, for instance as a bridge to a completely different level of mobility for the physically handicapped population. In this endeavor, numerous precautions must be integrated into the intelligence of the wheelchair, especially, one of the most significant safety concerns is predicting and maintaining the wheelchair stability by perceiving environment.

The geometric shape and the semantic information of the surroundings and objects/obstacles are crucial for the maneuvering stability of the wheelchairs. Towards the robust safety in on-road and off-road scenarios, effective 3D simultaneous localization and mapping (SLAM) of the environment must be performed to gather the perceptive data for the wheelchairs in a form from which analysis can be performed. There are two main challenges in this big picture challenge: accurately mapping the environment with large data noise levels present and representing the wheelchair and environment interaction. This research outlines a LiDAR-camera based 3D perception approach with algorithms that enables effective wheelchair stability predictions.

Keywords: LiDAR-Camera, SLAM, Terrain 3D Mapping, 3D Reconstruction, Mesh Mapping, Dynamic Model, Wheelchair Stability

II. 3D LiDAR-based terrain mapping

3D Mapping using SLAM

With regards to the odometry component of 3D mapping, there are two typical perceptive sensor-based odometry solutions: LiDAR and visual. With regards to visual-based odometry, through the use of RGB images landmarks in the environment can be tracked to provide an estimate of the sensor's pose in the environment. In a similar fashion, LiDAR-based odometry, such as using iterative closest point (ICP), tracks 3D landmarks or pointcloud updated pose for localization. A couple major limitations of visual odometry is the fact that it cannot be performed in a dark environment as it is dependent upon RGB image information and without light there is no data.

In this paper, with the world's smallest high-resolution LiDAR camera Intel® RealSense™ L515, a LiDAR-based odometry was fused with onboard inertial measurement unit (IMU) sensor for pose tracking and mapping, by leveraging a real-time appearance-based (RTAB) mapping approach. The essence of RTAB mapping is that at each node, the corresponding depth pose of the sensor , x_i, and the raw data, D, at a specific time step t, while a link contains the measurement constraints w_t and v_t. The constraints at time step t, for pose x_t and sensor reading, z_t, are given by,

$$v_t = z_t - h(x_t, m_t) \tag{1}$$

$$w_t = x_t - g(x_{t-1}, u_t) \tag{2}$$

where h() and g() represent the measurement and motion functions and Q_t and R_t are the covariances of the measurement and motion noise. Then the optimal graph configuration can be solved by minimizing the following relation,

$$J_{graphSLAM} = x_0^T{}_0 + \sum_t w_t^T R_T^{-1} w_t + v_t^T Q_T^{-1} v_t \tag{3}$$

The goal of graph SLAM is to create a graph of all robot poses and features encountered in the environment and compute the most likely robot's path and map of the environment.

VI. Future Research

A future area of improvement in our work is the running time for the mesh generation. Although, Poisson reconstruction was selected due to it's distinct characteristic of being resistant to data noise, it presents a poor time complexity that in this paper was dealt with by subsampling the 3D pointcloud. Also, another interesting area to investigate is the influence of other terramechanical properties of terrain on stability of wheelchairs. The vision of this work is to be integrated into a comprehensive autonomous wheelchair to help enable greater independence/mobility for handicapped populations.

III. 3D Mapping Stability Prediction Pipeline

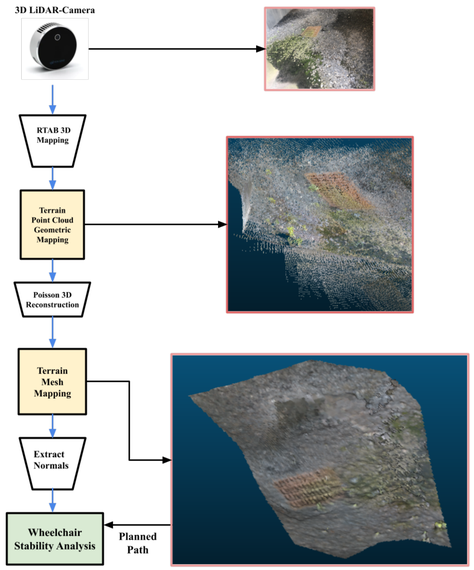

Figure 1: Terrain LiDAR-camera 3D mapping and stability analysis for wheelchair

IV. Experiment Design

In this section we outline the experiment in which the proposed algorithm (Figure 1) was used to generate a 3D triangular mesh to represent a variety of different terrains/obstacles that could be seen by an autonomous wheelchair in an urban environment. These terrains fell into two categories: traversable and non-traversable. Simulations in ADAMS were performed to verify our hypothesis surrounding whether the wheelchair could handle certain geometric characteristics of a terrain.

Field Data Collection Setup

For the data collection using the L515, we implemented the SLAM based 3D mapping approach outlined above to construct maps of various terrains deployed on the wheelchair shown in Figure 2.

Figure 2: Automated wheelchair equipped with visual sensors for experiments

The wheelchair, is equipped with an outward facing L515 LiDAR camera for data collection of the environment in addition to a D435i RGB-D camera facing the user for human-machine interaction purposes. In this paper, the LiDAR camera sensor was used to map a wide variety of terrains to evaluate the various components of the proposed pipeline including: mesh quality, stability prediction, and odometry. The wheelchair runs Ubuntu 16.04 with ROS kinetic, therefore the pipeline was deployed on that system.

Dynamic Simulation Design

Establish the dynamic model of wheelchair in ADAMS/View, with a three-dimensional size of the wheelchair (length × width × height) of $1100 \times 700 \times 1300\ mm$, The wheelbase B of the wheelchair is $600\ mm$, the wheelbase L of the wheelchair is $560\ mm$, and the wheelchair's height of the mass centroid from the ground h_s is $440\ mm$ as well as other parameters. In this case, 3D equivalent volume pavement is selected for simulation pavement, make the real road elevation data collected by the above laser radar into a .rdf road file, Import ADAMS/View to generate 3D road simulation model. as seen in Figure 3.

Figure 3: Wheelchair simulated model for stability prediction evaluation

V. Experimental Results

3D Mapping and Reconstructed Mesh Results

In order to evaluate the quality of the various mesh generation techniques, edge root mean square (ERMS) in formula (4) was used as the quality metric,

$$ERMS_\mu = \frac{1}{N} \sum_{t \in \Lambda_t} \sqrt{\frac{t_{L1}^2 + t_{L2}^2 + t_{L3}^2}{3}} \tag{4}$$

where Λ_T is the set of all triangles that make up the different meshes, and t_{L1}, t_{L2}, t_{L3}, are the legs of triangle $t \in \Lambda_t$. N is also the number of triangles in a given mesh.

As shown in Table 1, it indicates that Poisson reconstruction produced mesh representations that were an effective representation for the 3D map while keeping the geometric characteristics of the data (Figure 1).

Table 1: Performance of LiDAR-camera data mesh generation algorithms

Edge Root Mean Square				
K	0.5	0.7	0.9	0.97
Poisson reconstruction | $O(m^3 log(m))$				
μ	0.00634	**0.00455**	0.00411	0.00419
σ	0.004	**0.003**	0.002	0.002
Alpha Shapes | $O(m^2)$				
μ	0.01522	0.01443	0.01198	0.00929
σ	0.014	0.013	0.012	0.012
Delaunay Triangulation | $O(mlog(m))$				
μ	0.02197	0.02388	0.024193	0.02394
σ	0.052	0.049	0.049	0.051

The result shows that even when the 3D map data is gathered from a LiDAR sensor, Poisson reconstruction is still by far the most optimal mesh generation algorithm among the ones tested.

Odometry Results and Comparison

In order to evaluate the effectiveness of the odometry using the data gathered by the LiDAR camera sensor, a circular route was driven in an indoor environment. From there we are able to visualize the amount of drift that each odometry technique presents without the use of loop closure detection.

The results can be visualized in Figure 4 for the same trajectory data. The LiDAR-inertial odometry shows more accurate close-loop pose tracking, while the visual-inertial odometry has larger draft in terms of the start/end points which are two sides of an reference board object.

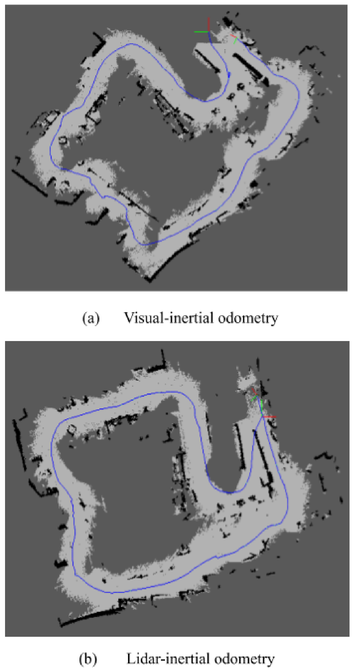

(a) Visual-inertial odometry

(b) Lidar-inertial odometry

Figure 4: Tracked poses from environmental landmarks using a LiDAR camera

Dynamic Simulation Results

As shown in Figure 5, the variations in the acceleration (first row), posture angle (second row) and normal forces (third row) demonstrate the anti-tipping characteristic of the wheelchair in the simulated environment.

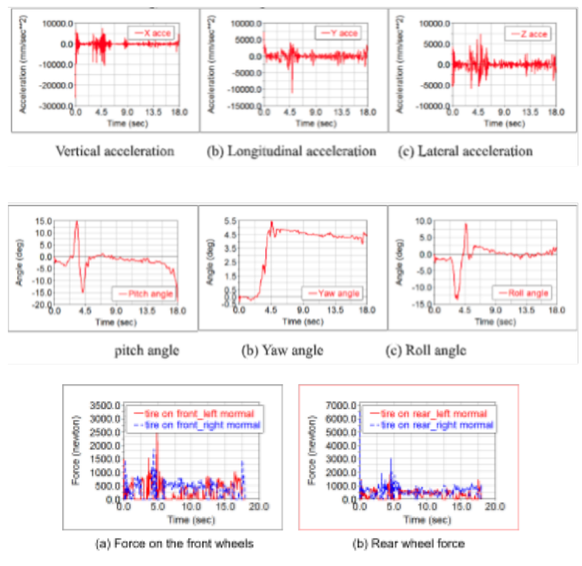

Figure 5: Dynamic simulation results for posture angle (first row) centroid acceleration (second row) as well as normal forces (third row) of an automated wheelchair

All three charts have similar trends in the sense that while driving over the initial flat road the values were relatively steady compared to the fluctuations caused by traversing the curb as well as the rugged terrain behind the curb.